

Article

Testing and Fatigue Life Assessment of Timber Truck Stanchions

Filip Lisowski ^{1,*}  and Edward Lisowski ²¹ Institute of Machine Design, Cracow University of Technology, Warszawska 24, 31-155 Cracow, Poland² Institute of Applied Informatics, Cracow University of Technology, Warszawska 24, 31-155 Cracow, Poland; edward.lisowski@pk.edu.pl

* Correspondence: filip.lisowski@pk.edu.pl

Received: 4 August 2020; Accepted: 31 August 2020; Published: 3 September 2020



Abstract: Components of transport trucks are subjected to dynamic cyclic loads. The magnitude of these loads depends on road conditions and cargo mass. Cyclic loads can cause fatigue failure at stress levels significantly below the yield strength of the material. When calculating fatigue, it is necessary to determine the actual loads acting on the structure under working conditions. In this study, stanchion displacements of overloaded timber trucks were measured under both static and dynamic loads. For the specified mass of timber, a history of dynamic loads acting on the stanchion was obtained. Then, based on the finite element analysis, stress concentration points were determined within the base material and welded joints of the stanchion. The history of maximum stresses at concentration points was determined. Stress ranges and mean stresses for the load history were calculated using the rainflow fatigue cycle counting method. Repeats to failure were determined on the basis of the Palmgren–Miner cumulative damage rule and the modified Goodman correction for the points with the highest stress level. Experimental investigation of the actual load history of the stanchion of significantly overloaded timber truck allowed to determine the mileage to potential failure.

Keywords: truck stanchions; fatigue life; cumulative damage

1. Introduction

Timber trucks are commonly used to transport logs on both forest and public roads. Transportation is the most expensive part of the timber production process. The relationship between the volume of timber cargo and its actual weight can be difficult to accurately determine. According to statistical studies, up to 60–80% of timber truck sets in European countries can be overloaded. This means that the timber cargo is heavier than can be carried by the truck within the cargo volume. In such cases, the permissible total weight of a timber truck set can be exceeded by up to 50% [1]. The possibility of significant overload makes it advisable to include it in the design process of truck components. It is particularly important to determine the actual load history for fatigue calculations. In general, the assessment of the fatigue life of structural components is based on determining stress amplitudes and mean stresses and considering S–N diagrams of the materials. The load history for the design process can be accepted with constant amplitude according to standardized load histories (SLHs) or based on measurements under service loads. For load cycles that are not fully reversed, mean stress correction is required [2]. Problems related to fatigue life prediction of constructional elements were raised by authors of numerous publications. Będkowski provided a historical outline of fatigue analysis and described current trends in assessing the fatigue life of engineering structures under service loads [3]. Classification criteria of fatigue failure and stress state components for multiaxial load conditions were also discussed. Mrzygłód and Zieliński [4] and Mrzygłód [5] presented problems related to the numerical implementation of multiaxial high-cycle fatigue criteria in structure

optimization. An original method of calculating fatigue life of a soldered construction node based on the two-parameter fatigue characteristics and the linear cumulative damage hypothesis was developed by Szala [6]. Armentani et al. presented findings in [7] on the fatigue behavior of single multiple-riveted lap joints used for aeronautic structures. Both the fatigue life and critical crack size were analyzed. Romanowicz and Szybiński delivered analytical formulas in [8] for determining stresses in the contact area and proposed a methodology for fatigue life assessment of rolling bearings by applying the multiaxial high-cycle fatigue hypothesis. In [9], Romanowicz presented a numerical evaluation of the fatigue load capacity of the cylindrical crane wheel. The application of multiaxial high-cycle fatigue criteria for analyzing the subsurface rolling contact fatigue of structures working in contact conditions was discussed. Studies by Savkin et al. [10] and Jadav et al. [11] referred to the fatigue analysis of truck frames under service loads. In turn, dynamic loads resulting from the actual road roughness were considered in the truck frame fatigue analysis by Zehsaz et al. [12].

Experimental tests are crucial for fatigue failure analysis. These tests may concern the collection of load history data or the execution of fatigue tests for specified load sequences. For example, Yuan et al. presented findings on the fatigue life assessment of a wheel loader [13]. The history of external loads was obtained on the basis of experimental tests involving strain gauge measurements and the load identification model. A cumulative damage theory and a structural stress method were applied to determine the fatigue life of welded components. In the study by Han et al., the method of fatigue strength evaluation of a bogie frame was proposed [14]. Analysis included calculations of cumulative fatigue damage and experimental verification on a full-scale test rig. In addition, an increase in the dynamic factor was assumed in the following fatigue test sequences. Meanwhile, a fatigue life prediction of the end beam of a freight car bogie was developed in the study by Baek et al. [15]. Finite element stress analysis and the fatigue damage prediction based on the rainflow cycle counting method were involved. Load sequences obtained from measurements during starting and braking were used for fatigue tests on the test bench. In [16], Witek presented the analysis of compressor blades subjected to high-cycle fatigue. The study involved the numerical determination of stresses and crack initiation analysis after damage caused by a foreign object. Finite element results were compared with experimental vibration tests. Song et al. presented research on the fatigue life assessment of the purified terephthalic acid filter press of welded shell structure [17]. The tested pressure was determined by experimental analysis, while the finite element method was used for fatigue life calculations and optimization. The thermomechanical model and high-cycle regime were considered. Both the fatigue strength reduction method and the hot-spot method were used to assess the fatigue life of welded joints.

In this paper, the fatigue life of timber truck stanchions operating under significant overload conditions was examined. Experimental tests were carried out to determine the actual loads acting on the stanchion. Then, based on finite element analysis, weak points of the structure and the corresponding stress history were determined. By applying a modified Goodman mean stress correction and the Palmgren–Miner cumulative damage rule, the life to failure of the stanchion was determined.

2. Experimental Load History Data Collection

An experiment was conducted under operating conditions in order to determine the actual load history of a single stanchion. Two pairs of stanchions with a nominal load of 50 kN were used in tests on local roads. Figure 1 shows the timber truck before the cargo was loaded, and Figure 2 shows the truck during timber loading. Direct measurements of the forces acting on particular points of the stanchion are rather problematic. Therefore, it was decided to measure the transverse displacement of the free end of the stanchion and determine the forces based on the assumed distribution of masses and dimensions of the logs. The measuring system consisted of a displacement transducer mounted on a support fixed to an additional unloaded stanchion and a rigid beam mounted on the loaded stanchion as shown in Figure 3.



Figure 1. View of the truck stanchions with the displacement transducer before the timber was loaded.



Figure 2. View of the truck during timber loading.



Figure 3. Displacement transducer mounted on the unloaded stanchion.

The data recorder was placed in the truck cab. The timber truck was loaded with logs and then weighed. The static load was 140 kN, and thus the static overload was 40%. The measured transverse displacement of the free end of the stanchion under a static load was 75 mm. The load

distribution per stanchion determined for a static load case is shown in Figure 4. Loads caused by logs that were not in direct contact with the stanchion were also included. Forces for dynamic load cases were determined by multiplying the forces obtained for the static load by the coefficient related to the transverse displacement of the free end of the stanchion. This coefficient is defined as $k = x_{dyn}/x_{stat}$, where x_{dyn} stands for the transverse displacement under dynamic load and x_{stat} stands for the transverse displacement under static load. The load history obtained from the experiment is shown in Figure 5.

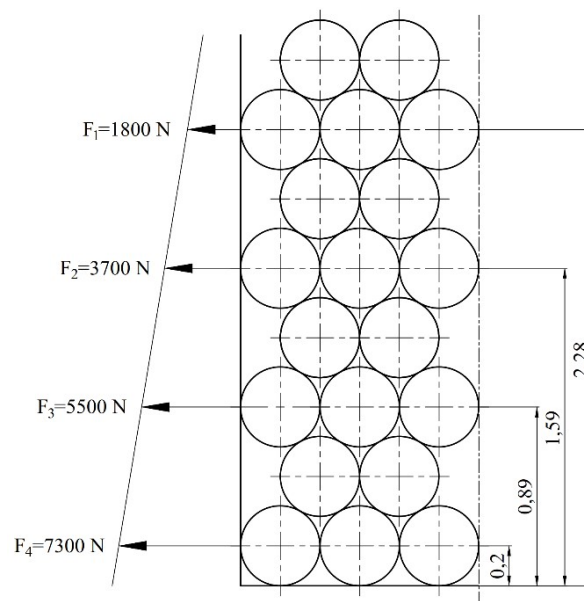


Figure 4. Log arrangement and static load distribution on the stanchion (dimensions in meters).

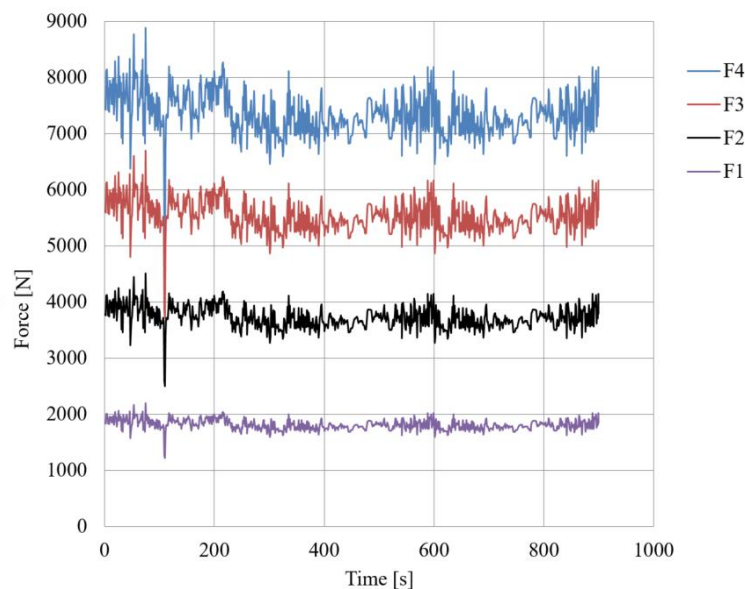


Figure 5. Load history obtained from the experiment.

3. Finite Element Analysis

Calculations applying finite element analysis were carried out using ANSYS Mechanical software [18]. A finite element model of the stanchion was prepared to identify stress concentration points in the structure and to determine the stress history for these points. The model consisted of 38,384

high-order shell elements generated within mid-surfaces of the stanchion components. The geometry of the welds was also included. Contact elements were defined between the socket and the stanchion beam. The rigid contact was set for a pair of surfaces where the beam and the socket were rigidly bolted. On the other interfaces, the contact with friction was defined. A friction coefficient of 0.15 was assumed. S355J2 structural steel with yield strength of $R_e \geq 355$ MPa was selected as the material of the stanchion. The finite element model of the stanchion is shown in Figures 6 and 7.

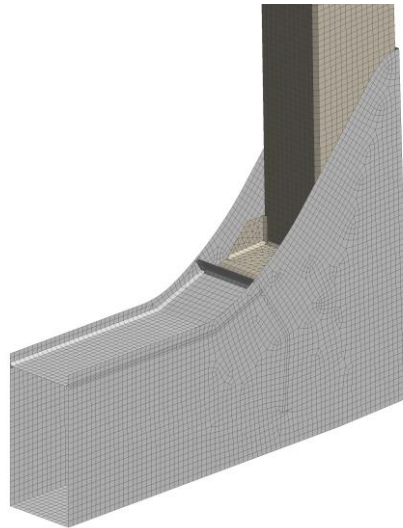


Figure 6. Finite element model of the stanchion: view of the socket.

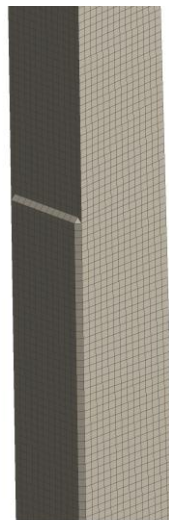


Figure 7. Finite element model of the stanchion: view of the reinforcement plate.

Stress concentration points were determined based on the von Mises stress distribution under the static load as presented in Figure 8. Points 1 and 2 were identified within weld toes of fillet welds at the end of the reinforcement plates on a rectangular hollow section. Point 3 was found within the toe of a two-sided fillet weld, whereas points 4–6 were selected within the base material. The history of the maximum values of appropriate stress components for further fatigue analysis was determined for each of the above points. Maximum normal stress in the direction of tension was considered for concentration points within the base material. In turn, structural hot-spot stress for welded joints was determined according to the methodology presented in [19]. Assuming relatively coarse mesh with element size equal to material thickness t , hot-spot stress σ_{hs} within the weld toe was approximated

using Equation (1), where $\sigma_{0.5t}$ and $\sigma_{1.5t}$ stand for stresses in reference points located $0.5t$ and $1.5t$ away from the weld toe as shown in Figure 9.

$$\sigma_{hs} = 1.5 \cdot \sigma_{0.5t} - 0.5 \cdot \sigma_{1.5t} \tag{1}$$

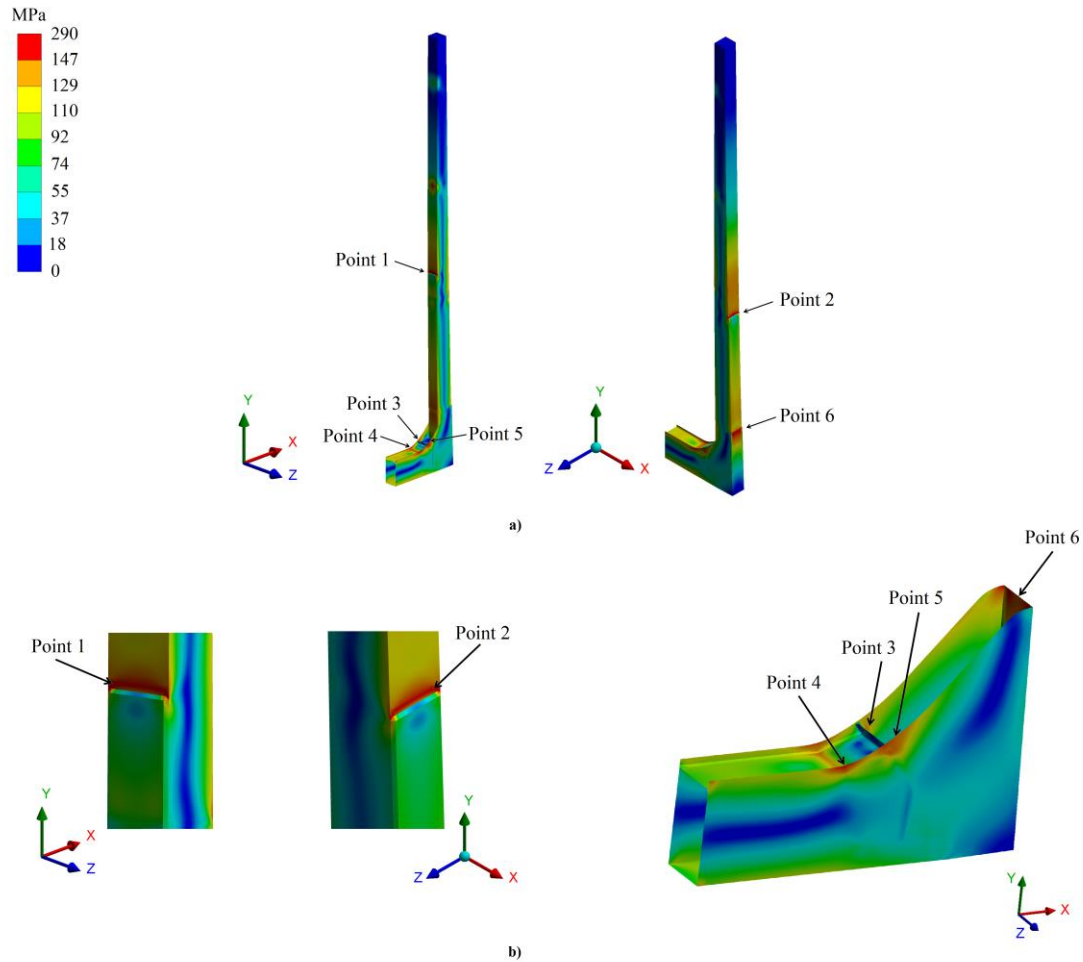


Figure 8. Von Mises stress distribution and stress concentration points under static load: (a) general views; (b) detailed views.

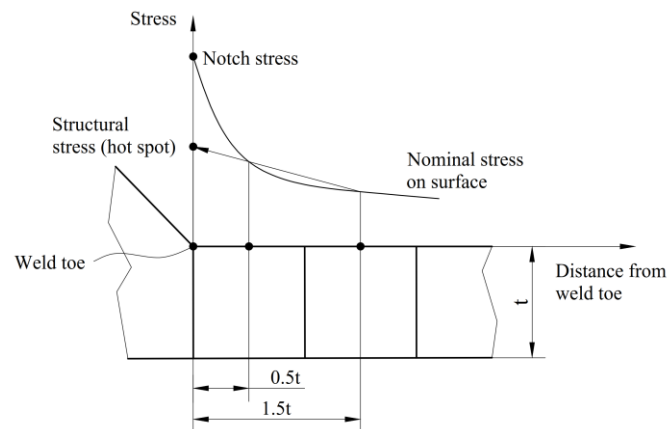


Figure 9. Hot-spot stress extrapolation.

The history of maximum hot-spot stress under dynamic load is shown in Figure 10, while maximum normal stress in stress concentration points within the base material is shown in Figure 11.

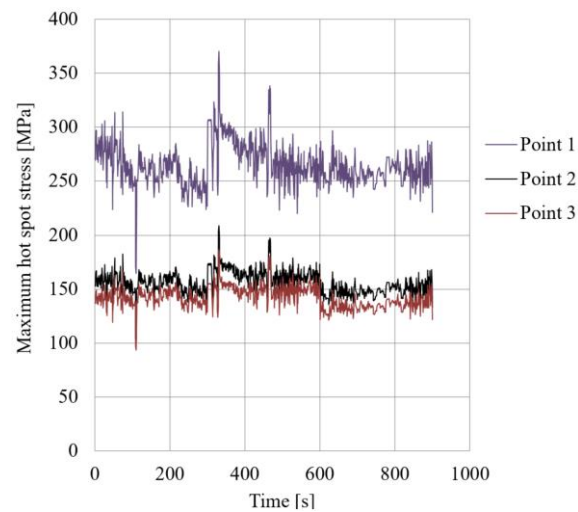


Figure 10. History of maximum hot-spot stress within the welds under dynamic load.

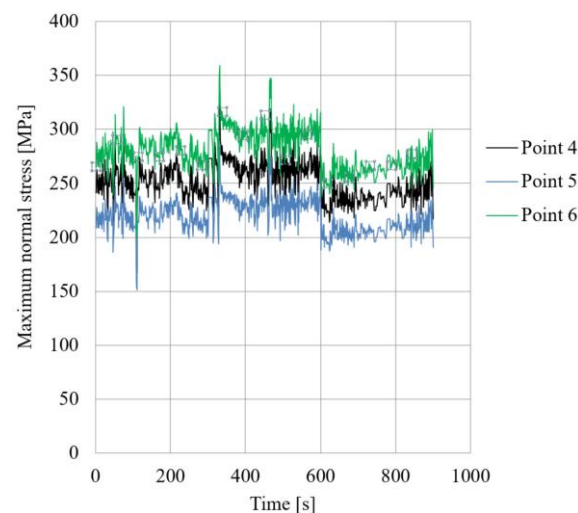


Figure 11. History of maximum normal stress within the base material under dynamic load.

4. Fatigue Analysis

4.1. Rainflow Cycle Counting Method

The rainflow fatigue cycle counting method is used in fatigue analysis to reduce the spectrum of varying stress and obtain simple stress reversals [20]. This method is compared to the rain running down a pagoda roof. The algorithm for counting half-cycles is defined as follows:

1. The stress history plot is rotated by 90° to reflect the direction of the rain that is falling down.
2. Rainflow starts at each successive point of the extreme.
3. Stress reversals are defined with the assumption that rain falls until one of the following conditions is met:
 - a. It drops on the opposite larger maximum or smaller minimum point;
 - b. It meets another flow;
 - c. It falls outside the roof.

Concerning the example of a simple stress history shown in Figure 12, the cycle counting algorithm is as follows:

1. The stress history plot is rotated by 90° so that Figure 13 is obtained.
2. Point A is identified as the largest peak in the stress history.
3. A–F is identified as the first largest reversal.
4. F–I is identified as the second largest reversal.
5. Within the first largest reversal A–F:
 - a. B–E reversal is identified.
 - b. E–B reversal is identified.
 - c. C–D reversal is identified.
 - d. D–C reversal is identified.
6. Within the second largest reversal F–I:
 - a. G–H reversal is identified.
 - b. H–G reversal is identified.

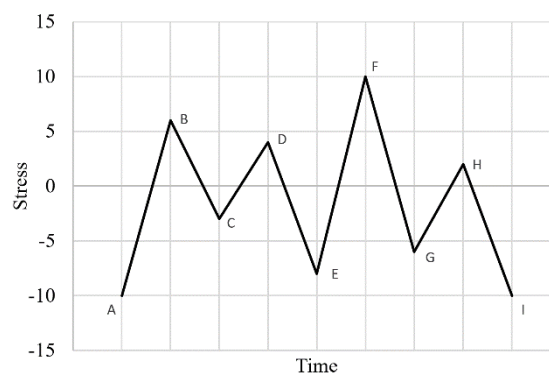


Figure 12. Sample stress history.

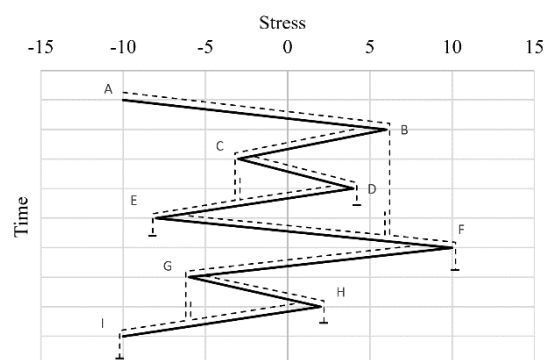


Figure 13. Stress history (rotated by 90°).

The spectrum of varying stresses obtained from finite element analysis was reduced by applying the above technique. For the analyzed timber truck stanchions, equivalent sets of simple reversal stress cycles were obtained. The effect of stress reduction is presented in Figure 14. Histograms obtained for all the points under consideration include information about the number of reversal stress cycles, corresponding mean stress and stress range. The highest mean stress and the highest stress range are observed from Point 1.

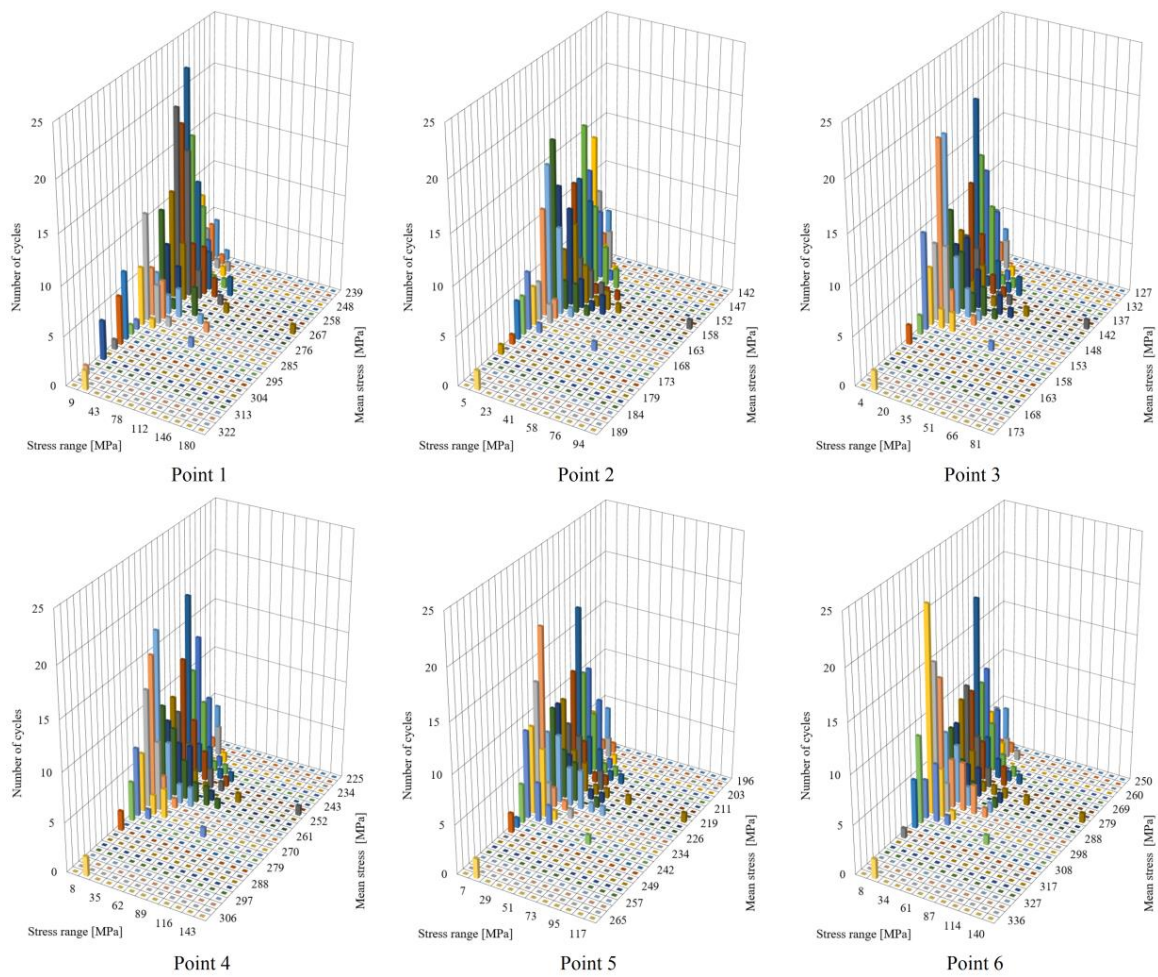


Figure 14. Rainflow cycle counting histograms of reversed stress cycles at concentration points.

4.2. Fatigue Life Calculations

In order to estimate the fatigue life of the stanchion, cumulative fatigue damage and repeats to failure were calculated using the Palmgren–Miner rule [21]. The cumulative damage D is given by Equation (2). Value N_i is the fatigue strength obtained from S–N diagrams, whereas n_i indicates the number of cycles for the stress range. Repeats to failure were calculated as $R = 1/D$.

$$D = \sum_{i=1}^k \frac{n_i}{N_i} \tag{2}$$

Since stress cycles obtained as a result of spectrum reduction had non-zero mean stress, the Goodman correction was used when calculating fatigue strength. The modified Goodman relation is given by Equation (3), where σ_a and σ_m stand for stress amplitude and mean stress, σ_u is ultimate tensile strength and σ_{Nf} indicates equivalent fully reversed stress.

$$\frac{\sigma_a}{\sigma_{Nf}} + \frac{\sigma_m}{\sigma_u} = 1 \tag{3}$$

Fatigue resistance S–N curves were accepted for the calculations in accordance with [19]. S–N curves are shown in Figure 15. Fatigue classes referred to the structural details as follows: FAT160 with unwelded parts, for which fatigue resistance was assessed based on nominal stresses, and FAT100

with two-sided fillet welds and fillet welds at the end of the reinforcement plates on a rectangular hollow section, for which fatigue resistance was assessed based on structural hot-spot stresses.

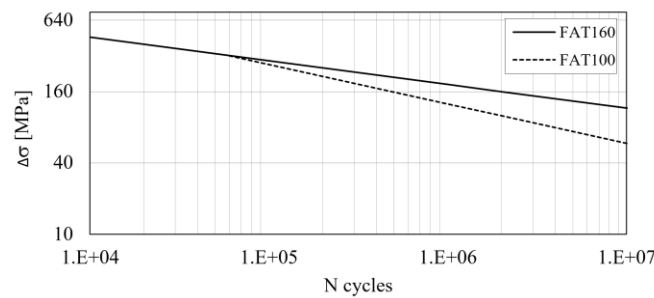


Figure 15. Fatigue resistance S–N curves [19].

The results of fatigue life calculations are presented in Table 1. An operating time was calculated by multiplying the number of repeats to failure by a single cycle time of 900 s. The mileage to failure was estimated under the assumption that the average vehicle speed is 50 km/h.

Table 1. Results of fatigue calculations.

	Repeats to Failure	Operating Time to Failure (h)	Mileage to Failure (km)
Point 1	84,420	21,105	1,055,250
Point 2	1,327,376	331,844	16,592,200
Point 3	3,095,003	773,751	38,687,538
Point 4	1,400,038	350,010	17,500,475
Point 5	7,182,869	1,795,717	89,785,863
Point 6	791,447	197,862	9,893,088

5. Discussion

The results of the fatigue life calculations revealed that the weakest point of the structure belongs to the weld toe of the fillet weld located at the end of the reinforcement plate on the rectangular hollow section. The analyzed region is under tensile stress. The fatigue life obtained for that point was more than 1 million kilometers. Such a result could be accepted as sufficient for the structure under consideration. However, the fatigue life obtained for Point 1 is at least one order of magnitude less than for the other stress concentration points under consideration. The fatigue class FAT100 is assigned to such a weld and is also assigned to the butt weld that could be alternatively considered. In addition, the fatigue strength is determined by the type of weld and not by the strength of the base material. Therefore, neither the use of the butt weld nor the use of steel with higher strength would change the results of fatigue life calculations for welded joints. In order to obtain comparable fatigue life within the entire structure of the stanchion, it is advisable to redesign the node to achieve higher fatigue strength. In the view of high possibility of stanchion overload, the removal of the weld from this location should be considered.

6. Conclusions

As a result of the experimental test, the load history was obtained for the timber truck stanchions operating under overload conditions of 40%. By applying the finite element analysis, stress concentration points were determined for both welded and unwelded components. For the six selected points, an actual stress history was determined. For the points within the base material, corresponding normal stress was considered, whereas for the points within welds, hot-spot stress was estimated. Fatigue calculations were carried out using the Palmgren–Miner rule and by applying the modified Goodman mean stress correction. The analysis resulted in the determination of the weakest point of the tested structure, which significantly affected the fatigue life under overload conditions.

Author Contributions: Conceptualization, F.L. and E.L.; methodology, F.L. and E.L.; software, F.L.; investigation, E.L.; writing—original draft preparation, F.L.; visualization, F.L. All authors have read and agreed to the published version of the manuscript.

Funding: This research received no external funding.

Conflicts of Interest: The authors declare no conflict of interest.

References

1. Trzciński, W.; Sieniawski, W.; Moskalik, T. Effects of timber loads on gross vehicle weight. *Folia For. Pol. Ser. A* **2013**, *55*, 159–167. [[CrossRef](#)]
2. Heuler, P.; Klätschke, H. Generation and use of standardized load spectra and load–time histories. *Int. J. Fatigue* **2005**, *27*, 974–990. [[CrossRef](#)]
3. Będkowski, W. Assessment of the fatigue life of machine components under service loading—A review of selected problems. *J. Theor. Appl. Mech.* **2014**, *52*, 443–458.
4. Mrzygłód, M.; Zieliński, A.P. Numerical implementation of multiaxial high-cycle fatigue criterion to structural optimization. *J. Theor. Appl. Mech.* **2006**, *44*, 691–712.
5. Mrzygłód, M. Two–stage optimization method with fatigue constraints for thin-walled structures. *J. Theor. Appl. Mech.* **2010**, *48*, 567–578.
6. Szala, G. Application of two-parameter fatigue characteristics in fatigue persistence calculations of structural components under conditions of a board spectrum of loads. *Pol. Marit. Res.* **2016**, *23*, 138–145. [[CrossRef](#)]
7. Armentani, E.; Greco, A.; De Luca, A.; Sepe, R. Probabilistic analysis of fatigue behavior of single lap riveted joints. *Appl. Sci.* **2020**, *10*, 3379. [[CrossRef](#)]
8. Romanowicz, P.J.; Szybiński, B. Fatigue life assessment of rolling bearings made from AISI 52100 bearing steel. *Materials* **2019**, *12*, 371. [[CrossRef](#)] [[PubMed](#)]
9. Romanowicz, P. Numerical assessment of fatigue load capacity of cylindrical crane wheel using multiaxial high-cycle fatigue criteria. *Arch. Appl. Mech.* **2017**, *87*, 1707–1726. [[CrossRef](#)]
10. Savkin, A.N.; Gorobtsov, A.S.; Badikov, K.A. Estimation of truck frame fatigue life under service loading. *Procedia Eng.* **2016**, *150*, 318–323. [[CrossRef](#)]
11. Jadav, C.S.; Panchal, K.C.; Patel, F. A review of the fatigue analysis of an automobile frames. *Int. J. Adv. Comput. Res.* **2012**, *2*, 103–107.
12. Zehsaz, M.; Morteza, H.S.; Etefagh, M.M.; Hassanneja, R. Fatigue strength of a chassis of a semi-heavy truck under dynamic loads due to real road roughness. *Trans. FAMENA* **2014**, *38*, 89–105.
13. Yuan, Z.; Ma, H.; Lu, Y.; Zhu, S.; Hong, T. The application of load identification model on the weld line fatigue life assessment for a wheel loader boom. *Eng. Fail. Anal.* **2019**, *104*, 898–910. [[CrossRef](#)]
14. Han, J.W.; Kim, J.D.; Song, S.Y. Fatigue strength evaluation of a bogie frame for urban maglev train with fatigue test on full-scale test rig. *Eng. Fail. Anal.* **2013**, *31*, 412–420. [[CrossRef](#)]
15. Baek, S.H.; Cho, S.S.; Joo, W.S. Fatigue life prediction based on the rainflow cycle counting method for the end beam of a freight car bogie. *Int. J. Automot. Technol.* **2008**, *9*, 95–101. [[CrossRef](#)]
16. Witek, L. Numerical stress and crack initiation analysis of the compressor blades after foreign object damage subjected to high-cycle fatigue. *Eng. Fail. Anal.* **2011**, *18*, 2111–2125. [[CrossRef](#)]
17. Song, M.; Zhang, W.; Jiang, W.; Wang, J.; Zhao, X.; Zhai, X. Fatigue life assessment of the shell structure of purified terephthalic acid filter press. *Materials* **2020**, *13*, 3276. [[CrossRef](#)] [[PubMed](#)]
18. *Ansys Academic Research Mechanical, Release 18.1*; ANSYS, Inc.: Canonsburg, PA, USA, 2017.
19. Hobbacher, A.F. *Recommendations for Fatigue Design of Welded Joints and Components*, 2nd ed.; IIW Document IIW-2259-15 ex XIII-2460-13/XV-1440-13; Springer International Publishing: Cham, Switzerland, 2016.
20. Matsuishi, M.; Endo, T. *Fatigue of Metals Subjected to Varying Stress*; Japan Society of Mechanical Engineering: Fukuoka, Japan, 1968.
21. Fatemi, A.; Yang, L. Cumulative fatigue damage and life prediction theories: A survey of the state of the art for homogeneous materials. *Int. J. Fatigue* **1998**, *20*, 9–34. [[CrossRef](#)]

